

Cold Consolidation of Ball-Milled Titanium Powders Using High-Pressure Torsion

KAVEH EDALATI, ZENJI HORITA, HIROSHI FUJIWARA, and KEI AMEYAMA

Pure Ti (99.5 pct) powders after processing with ball milling (BM) were consolidated to disc-shaped samples with 10-mm diameter and 0.8-mm thickness at room temperature using high-pressure torsion (HPT). A relative density as high as 99.9 pct, high bending and tensile strengths of 2.55 to 3.45 and 1.35 GPa, respectively, and a moderate ductility of 8 pct with an ultrafine grained structure are achieved after cold consolidation with HPT, which exceed those of hot consolidation methods. X-ray diffraction (XRD) analysis showed that a phase transformation occurs from α phase to ω phase during HPT under a pressure of 6 GPa as in bulk pure Ti, whereas no phase transformation is detected after processing with BM alone. It was confirmed that the strength and ductility are improved by a combined application of BM and HPT when compared with other severe plastic deformation methods applied to Ti and Ti-6 pct Al-4 pct V, so that no alloying elements are required for the achievement of a comparable strength and ductility.

DOI: 10.1007/s11661-010-0400-6

© The Minerals, Metals & Materials Society and ASM International 2010

I. INTRODUCTION

CONSIDERABLE interest in processing materials through the application of high-pressure torsion (HPT) has been allocated not only to produce ultrafine grained materials^[1] but also to consolidate powders^[2] as well as to achieve pressure-induced phase transformations.^[3] In the HPT process, first introduced by Bridgman in 1935,^[4] a small thin disc is placed between two massive anvils under a high hydrostatic pressure and intense shear strain is introduced by rotating the two anvils with respect to each other. The HPT as a processing tool for consolidation of powders was first used in 1991^[2] and further developed for the consolidation of metallic powders,^[5–8] composites,^[9–22] amorphous compounds,^[22–28] machining chips,^[28–30] and very recently for ceramic powders.^[31] The HPT process was also applied successfully as a cold consolidation technique without sintering process for ball-milled powders including pure Ni,^[5] pure Co,^[7] an Al-Mg alloy,^[8] Co-based metal-ceramic composites,^[17,18] and amorphous powders and chips.^[22,23,28]

It is well established that processing through the application of ball milling (BM), which is also known as mechanical milling and mechanical attrition, results in a severe grain refinement and a significant hardness increase.^[32,33] In BM, first developed by Benjamin

around 1966,^[32] a powder mixture is loaded into a mill along with grinding balls and the milling is conducted for a period of time. The ball-milled powders are then consolidated into bulk shapes using hot consolidation methods such as hot pressing, hot extrusion, hot isostatic pressing, hot roll sintering, spark plasma sintering, and spray forming followed by a sintering process.^[33] In spite of various publications regarding the BM of Ti,^[35–42] little attention has been paid to the cold consolidation of ball-milled Ti powders through the application of HPT.

Both BM and HPT may cause formation of metastable phases due to severe plastic deformation and high applied pressure. It is known that Ti exhibits a pressure-induced phase transformation from an α phase with the hcp crystal structure to an ω phase with the simple hexagonal structure during HPT and the ω phase is retained as a metastable phase at ambient pressure after unloading.^[34,35] The $\alpha \rightarrow \omega$ phase transformation in Ti was not detected after processing with BM, but instead, there is a report that Ti transforms from the α phase to an fcc phase by BM.^[37,38]

Thus, in this study, ball-milled Ti powders are subjected to consolidation using HPT, and the evolutions of mechanical properties and the occurrence of allotropic phase transformations are investigated under two different pressures as a function of the imposed strain.

II. EXPERIMENTAL MATERIALS AND PROCEDURES

This study used high-purity Ti (99.5 pct) powders with a particle size less than 45 μm having impurities of O 0.35, C 0.02, N 0.03, H 0.02, Fe 0.03, Mn 0.005, Mg 0.02, Cl 0.04, and Si 0.01 (wt pct). The Ti powders were

KAVEH EDALATI, Graduate Student, and ZENJI HORITA, Professor, are with the Department of Materials Science and Engineering, Faculty of Engineering, Kyushu University, Fukuoka 819-0395, Japan. Contact e-mail: kaveh.edalati@zaiko6.zaiko.kyushu-u.ac.jp HIROSHI FUJIWARA, Researcher, is with the Ritsumeikan Global Innovation Research Organization, Ritsumeikan University, Kusatsu 525-8577, Japan. KEI AMEYAMA, Professor, is with the Department of Materials Science and Engineering, Faculty of Science and Engineering, Ritsumeikan University.

Manuscript submitted December 17, 2009.

Article published online September 8, 2010

subjected to BM using a planetary device with a tungsten carbide vial for 50 hours with a rotation speed of 200 rpm. The ball-to-powder weight ratio was 1.8:1 and the material of balls was a high carbon chromium steel (JIS G4805/SUJ2). The vial volume and the ball diameter were 500 cm³ and 10 mm, respectively. To reduce the powder contamination and to avoid the atmosphere-induced structural evolution, as reported earlier,^[33–36] milling was conducted under pure argon atmosphere.

HPT was conducted at room temperature using the ball-milled Ti powders to consolidate to discs with dimensions of 10-mm diameter and 0.8-mm thickness under the pressures of 2 and 6 GPa and, subsequently, to introduce strain through either $N = 1, 4, 10,$ or 40 revolutions with a rotation speed of $\omega = 1.0$ or 0.2 rpm. Moreover, additional HPT experiments were conducted under the pressure of 6 GPa for $N = 10$ revolutions at a rotation speed of $\omega = 1.0$ rpm on powder samples without BM as well as a bulk sample both with the same purity of 99.9 pct. The details of HPT facility were reported elsewhere.^[46,47]

The HPT-processed discs were evaluated using Vickers microhardness measurement, bending test, tensile test, optical microscopy (OM), scanning electron microscopy (SEM), X-ray diffraction (XRD) analysis, transmission electron microscopy (TEM), and density measurement. First, after processing by HPT, the 10-mm discs were polished to a mirrorlike surface, and the Vickers microhardness was measured with an applied load of 200 g for 15 seconds along the radii from the center to edge at 8 different radial directions with 0.5-mm increments, as depicted by cross marks in Figure 1(a). Second, for bending test, miniature rods with a 0.5×0.5 mm² square cross section and 9-mm length were cut from the 10-mm-diameter discs at 1 mm away from the disc center, as illustrated in Figure 1(a). Three-point bending tests were carried out at room temperature to measure the bending load and displacement. The load was applied in the radial direction and the pressing direction for the samples processed by HPT

at 2 GPa for 10 revolutions. The supporting span was 8 mm and the stroke was controlled at a crosshead speed of 0.5 mm/s. Assuming linear elasticity, the bending stress, σ , was calculated from the load and the specimen geometry through the Euler–Bernoulli beam theory:^[48]

$$\sigma = \frac{3Fl}{2bh^2} \quad [1]$$

where F is the bending load, l is the supporting span (8 mm), b is the bending specimen width (0.5 mm), and h is the bending specimen height (0.5 mm). Third, miniature tensile specimens having 1.5-mm gage length, 0.7-mm width, and 0.5-mm thickness were cut from the 10-mm discs at the position 2 mm away from the center, as illustrated in Figure 1(a). Since the machining may introduce surface defects and may affect tensile behavior of miniature specimens, the specimens were carefully polished to smooth surfaces following the machining. The appearance of the tensile specimen before testing is shown in Figure 1(b). Each tensile specimen was mounted horizontally on grips and pulled to failure using a tensile testing machine with an initial strain rate of 2×10^{-3} s⁻¹. To examine the reproducibility of tensile results, tensile tests were repeated twice or three times on different samples processed at the same HPT conditions. Fourth, SEM was performed at 20 kV for observation of fractographs of tensile specimens after failure. Fifth, for XRD, 3-mm discs were punched out from the 10-mm discs at 3.5-mm away from the center, as shown in Figure 1(a). The 3-mm discs were ground and polished mechanically to a thickness of 0.5 mm smoothly, and XRD was performed on these samples as well as on powders after BM using the Co K_α radiation at 40 kV and 36 mA in a scanning step of 0.02 deg and at a scanning speed of 0.4 deg/min. Sixth, for TEM, the 3-mm-diameter discs used for the XRD were ground mechanically to a thickness of 0.15 mm and further thinned with a twin-jet electrochemical polisher using a solution of 5 pct HClO₄, 25 pct C₃H₃(CH₂)₂CH₂OH, and 70 pct CH₃OH at 263 K (–10 °C) under an applied voltage of 15 V. TEM was performed at 200 kV for microstructural observation and for recording selected-area electron diffraction (SAED) patterns. Seventh, density was measured using the samples processed by HPT at 2 GPa for 10 revolutions including annealed bulk samples for comparison. Three samples were used for these measurements. Both sides of the disc samples were polished to a mirrorlike surface, and the density, ρ , was determined at 298 K (25 °C) by Archimedes' principle using an electronic balance with an accuracy of 0.1 mg through the following equation:

$$\rho = \frac{\rho_w m_a}{m_a - m_w} \quad [2]$$

where ρ_w is the density of water, ~ 1 g cm⁻³ at 298 K (25 °C), and m_a and m_w are the mass of sample in the air and water, respectively. To obtain the average, the density measurement was repeated using three different samples processed at the same HPT conditions.

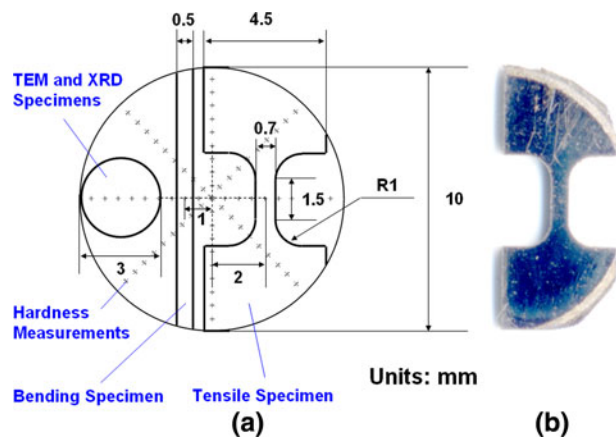


Fig. 1—(a) Schematic illustration of HPT disc and positions for microhardness measurements, and dimensions and locations for tensile and bending testing specimens and for TEM and XRD discs and (b) appearance of tensile specimen.

III. RESULTS

The measured values of microhardness are plotted in Figure 2 against the distance from the disc center for $N = 1, 4, 10,$ and 40 revolutions under (a) 2 GPa and (b) 6 GPa. It is apparent from Figure 2 that (1) hardness increases with the distance from the disc center for all numbers of revolutions for both pressures; (2) hardness increases with the numbers of revolutions under 2 GPa; (3) hardness increases from $N = 1$ to $N = 4$ under 6 GPa, but the hardness decreases for larger numbers of revolutions from $N = 4$ to $N = 40$; and (4) for the sample processed under 6 GPa for $N = 10$, the hardness level is higher for the rotation speed of $\omega = 0.2$ rpm when compared with $\omega = 1.0$ rpm.

All microhardness values in Figure 2 are plotted against the equivalent strain in Figure 3. Here, the nominal equivalent strain, ε , was estimated by the equation as^[1]

$$\varepsilon = \frac{2\pi r N}{\sqrt{3}t} \quad [3]$$

where r is the distance from the center of the disc, N is the number of revolutions, and t is the thickness of disc. It should be noted that the calculation of the equivalent

strain through Eq. [3] does not take into account the effect of slippage and thickness reduction during HPT processing, because the estimation of these factors is difficult for the form of powders.^[49,50] It is apparent from Figure 3(a) that the hardness increases with increasing equivalent strain at an early stage of straining under 2 GPa but appears to saturate to a level of 330 Hv at higher strains. Although some data points deviate from the delineated curve, the hardness variation with strain for powders consolidated by HPT is similar to that for bulk Ti processed by HPT.^[46] Two different saturation levels for hardness appeared for the pressure of 6 GPa, as shown in Figure 3(b): (1) 370 Hv for smaller numbers of revolutions or lower rotation speed and (2) 350 Hv for larger numbers of revolutions and higher rotation speed.

From the bending tests, the stress-displacement curves obtained with a crosshead speed of 0.5 mm/s for the samples processed for $N = 10$ under 2 GPa are delineated in Figure 4 for the radial direction and pressing direction as in the inset. The bending strength and the displacement to failure are large for the sample consolidated with HPT. The bending strength in the radial direction is higher than that in the pressing direction, but the total displacement to failure shows an opposite trend.

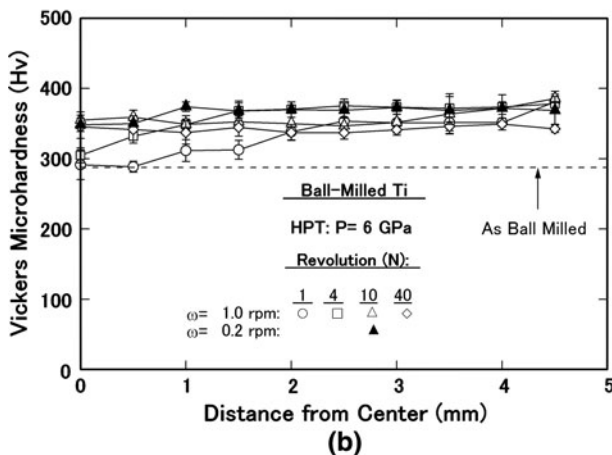
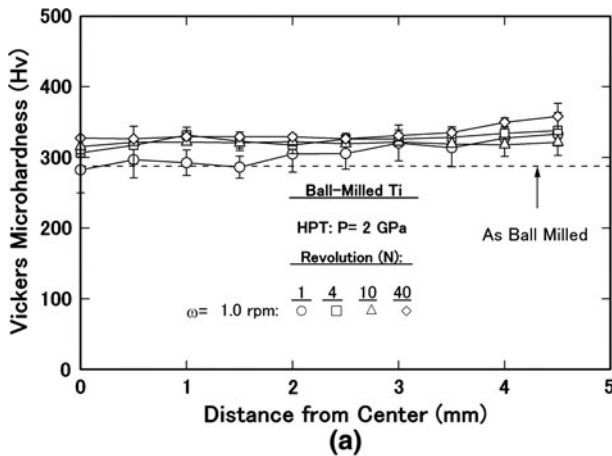


Fig. 2—Vickers microhardness plotted against distance from center for disc samples processed after various revolutions under (a) 2 GPa and (b) 6 GPa.

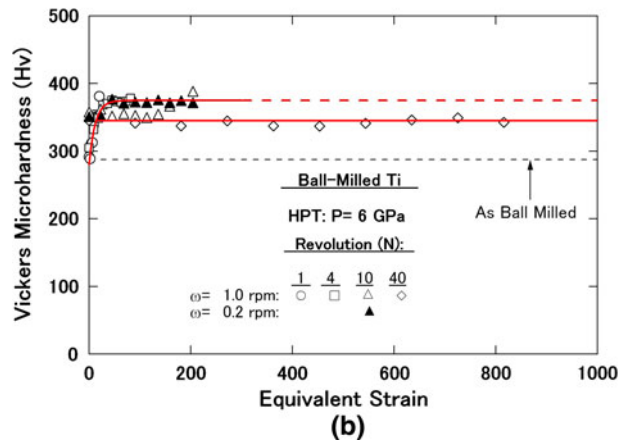
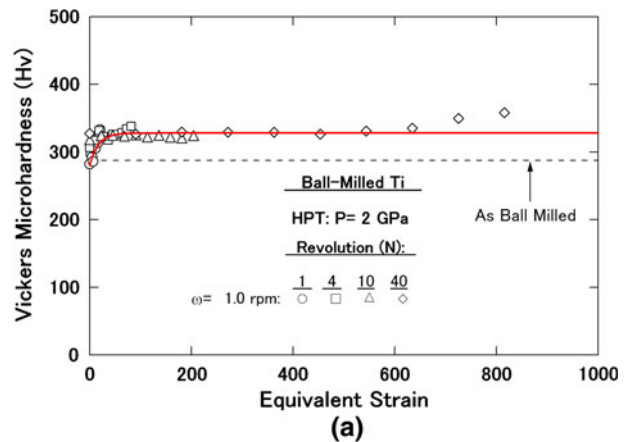


Fig. 3—Vickers microhardness plotted against equivalent strain for samples processed after various revolutions under (a) 2 GPa and (b) 6 GPa (all data points shown in Fig. 2).

Stress-strain curves for samples processed for different numbers of revolutions under (a) 2 GPa and (b) 6 GPa are delineated in Figure 5 from the tensile tests conducted at room temperature with an initial strain rate of $2 \times 10^{-3} \text{ s}^{-1}$. For the samples processed under 2 GPa, the tensile strength and the total elongation to failure increase from $N = 1$ to $N = 10$, but the elongation becomes almost zero at $N = 40$. For the samples

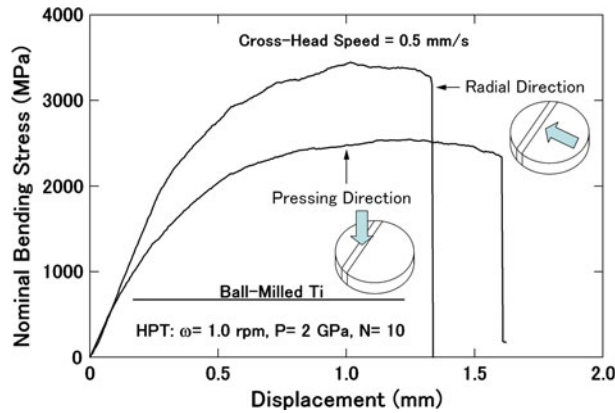


Fig. 4—Nominal bending stress vs displacement curves obtained from HPT discs processed for 10 revolutions under 2 GPa in the radial direction and pressing direction.

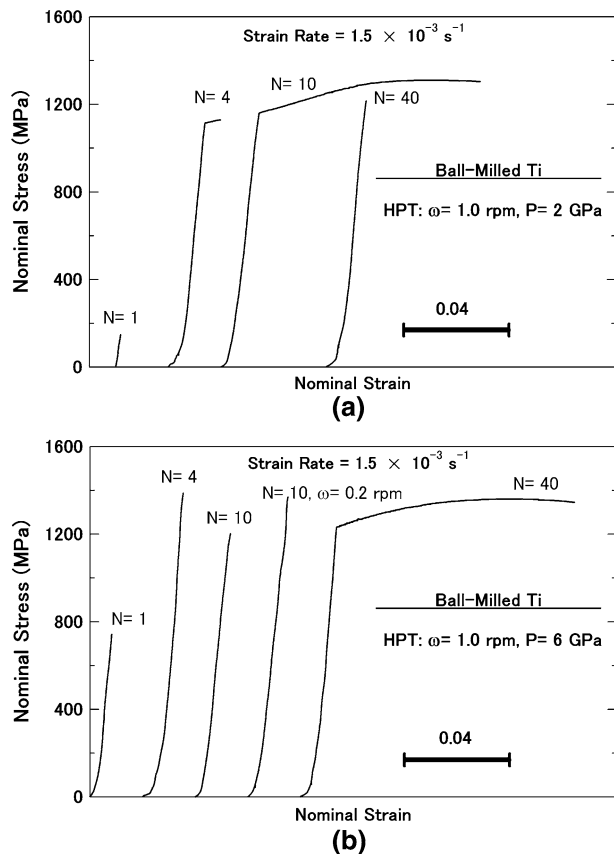


Fig. 5—Nominal stress vs nominal strain curves for samples processed after various revolutions under (a) 2 GPa and (b) 6 GPa.

processed under 6 GPa, the tensile strength increases from $N = 1$ to $N = 4$ but remains nearly constant above $N = 4$ up to $N = 40$, where all specimens except for $N = 40$ break elastically. Examination of Figure 5 indicates that the optimum conditions of HPT to achieve high strength and high ductility are, respectively, $N = 40$ under 6 GPa and $N = 10$ under 2 GPa.

The fracture surfaces after tensile testing of samples processed under 2 and 6 GPa are shown in Figures 6 and 7, respectively, where (a), (c), (e), and (g) are the overall views of the fracture surfaces corresponding to specimens processed for $N = 1, 4, 10,$ and 40 . Higher magnification views of the fractographs in (a), (c), (e), and (g) are shown on the right side in (b), (d), (f), and (h), respectively. The sample processed under 2 GPa for $N = 1$ fails due to crack propagation, as indicated by arrows (Figures 6(a) and (b)). The fracture surface changes to a veinlike pattern for $N = 4$, and some dimples associated with ductility are visible on the fracture surface, as marked by arrows (Figures 6(c) and (d)). The area fraction of the fine dimples increases in the sample processed for $N = 10$ (Figures 6(e) and (f)). The fracture occurs not only on a surface perpendicular to the tension direction but also on a surface having ~ 20 deg slope with respect to the tension direction, and the fracture surfaces appear to be smooth and cleaved for the sample processed for $N = 40$ (Figures 6(g) and (h)). All these fractographs are well consistent with the tensile testing results shown in Figure 5(a). The samples processed under 6 GPa for $N = 1, 4,$ and 10 have a veinlike pattern resulting in brittle fracture (Figures 7(a) through (f)), although some fine dimples are visible in the fracture surface after processing for $N = 10$. Fine dimple patterns are well developed for the sample processed for $N = 40$ (Figures 7(g) and (h)), indicating that the specimen breaks in a ductile manner. All these features presented in Figure 7 are consistent with the stress-strain curves shown in Figure 5(b).

TEM microstructures and the corresponding SAED patterns are shown in Figure 8 for samples after 10 revolutions under (a) 2 GPa and (b) 6 GPa. It is shown that the microstructures consist of ultrafine grains with grain sizes in the range of 50 to 300 nm and an average grain size of ~ 150 nm. Close examination of the microstructures reveals that there are many dislocations within the grains and most of the grains are surrounded by ill-defined grain boundaries. Whereas some elongated grains are observed in Figure 8(a), they are rarely seen in Figure 8(b). These microstructural features are similar to our earlier observations of bulk pure Ti after processing with HPT.^[46]

Figure 9 shows X-ray profiles for different numbers of revolutions under pressures of (a) 2 GPa and (b) 6 GPa. An examination of Figure 5 indicates the five important points.

- (1) No phase transformation is detected after processing of powders with BM even after 50 hours milling, and this is not consistent with published articles reporting a formation of fcc Ti during BM.^[37,38] The difference must be due to lower milling intensity and less contamination level in this study.

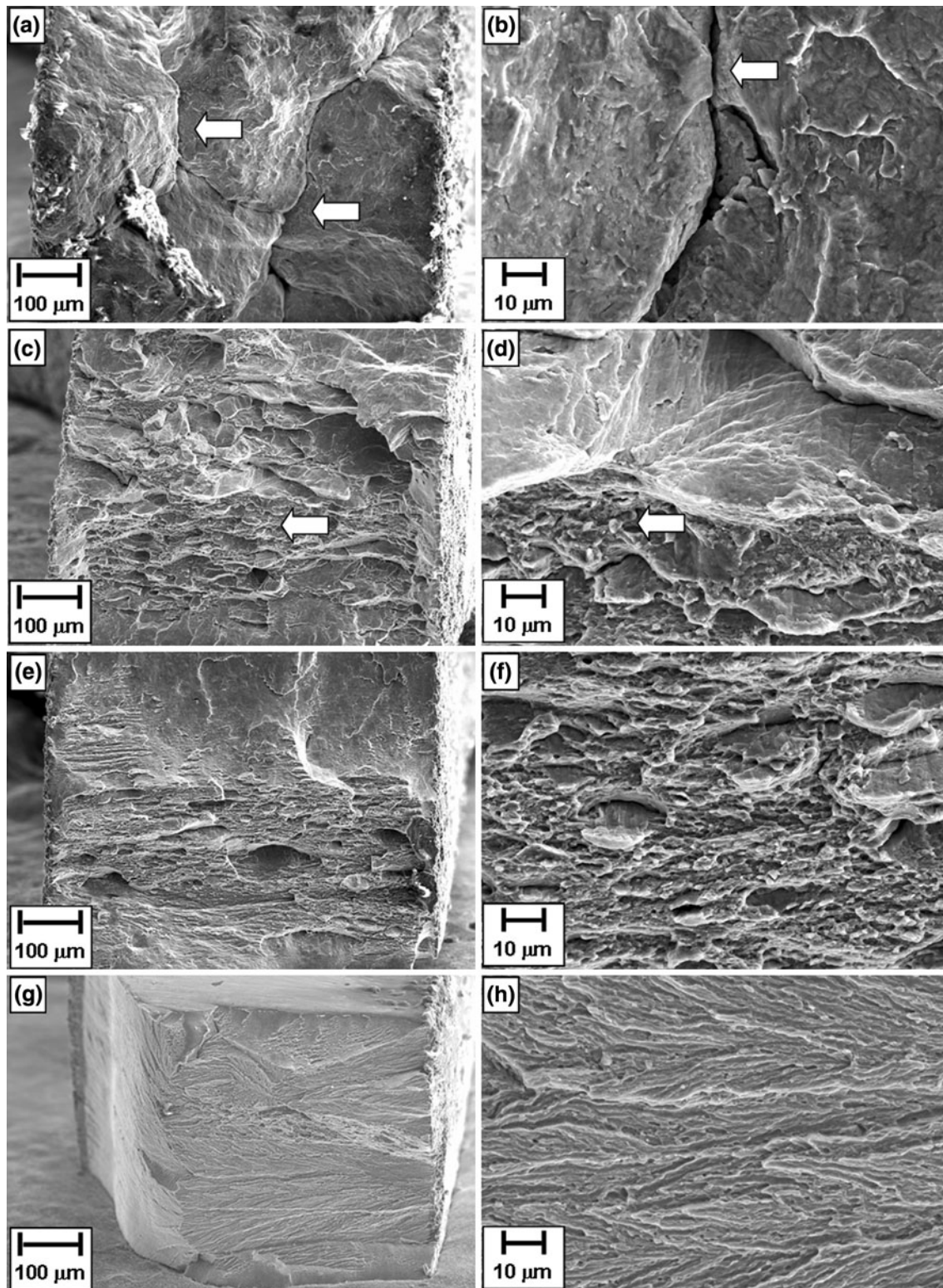


Fig. 6—SEM fractographs of samples processed under 2 GPa for $N =$ (a) and (b) 1, (c) and (d) 4, (e) and (f) 10, and (g) and (h) 40 revolutions.

(2) No phase transformation is detected after consolidation of powders with HPT under 2 GPa. However, a peak for the ω phase clearly appears after HPT for $N = 1$ under 6 GPa. This is in good agreement with earlier observations on bulk Ti

that an $\alpha \rightarrow \omega$ phase transformation occurs when HPT is operated under pressures higher than 3 to 4 GPa.^[43–46]

(3) A comparison between the peak height of $(1011)_z$ and $(0002)_z$ planes indicates that a texture develops

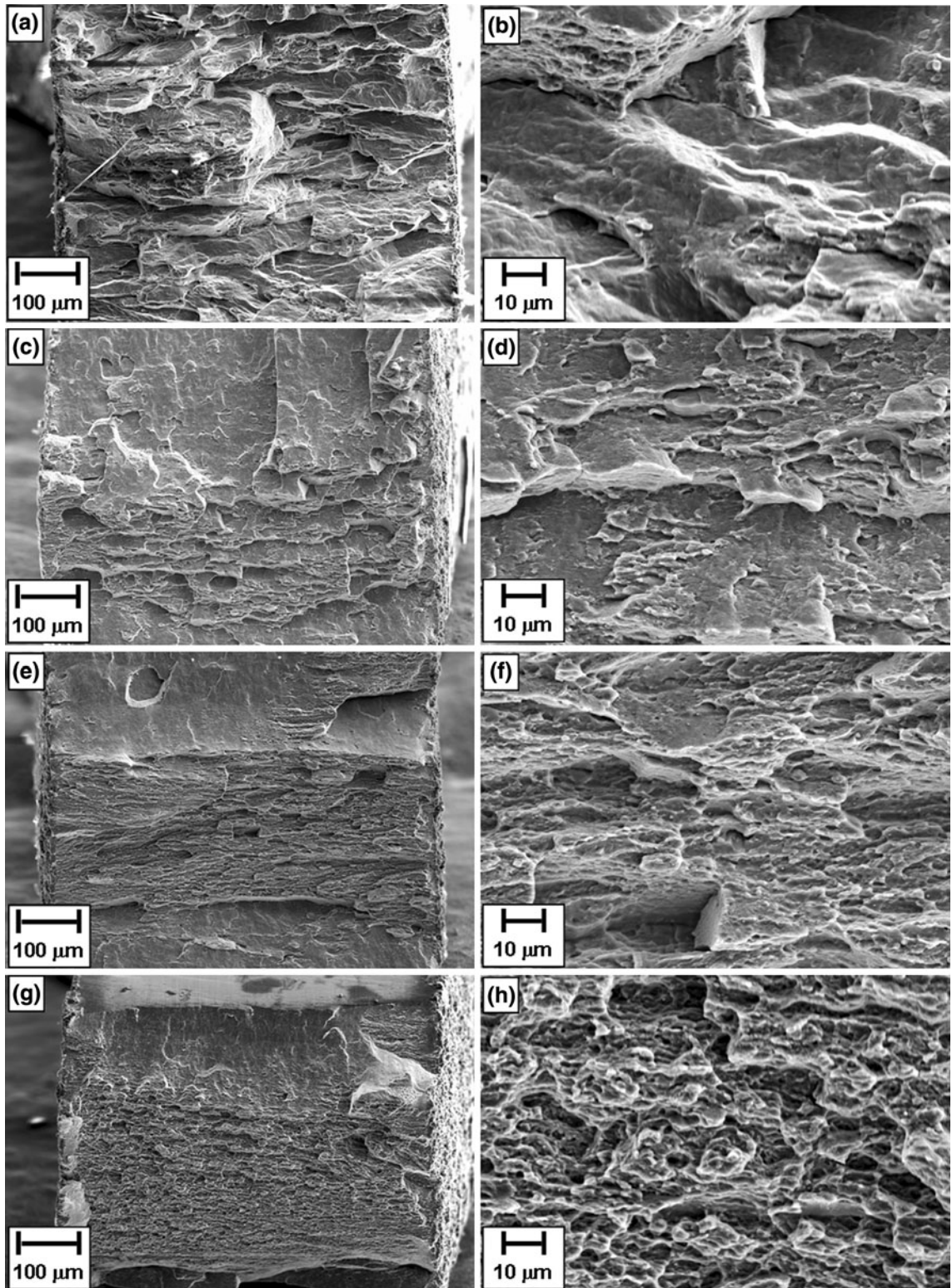


Fig. 7—SEM fractographs of samples processed under 6 GPa for $N =$ (a) and (b) 1, (c) and (d) 4, (e) and (f) 10, and (g) and (h) 40 revolutions.

such that the peak height of basal plane decreases with straining. Since the XRD analysis was performed in a direction perpendicular to shear plane, it is concluded that the pyramidal planes of the α

phase tend to be parallel to the shear plane and disc surface.

(4) The peak height of ω phase increases from $N = 1$ to $N = 4$ consistent with earlier works that the

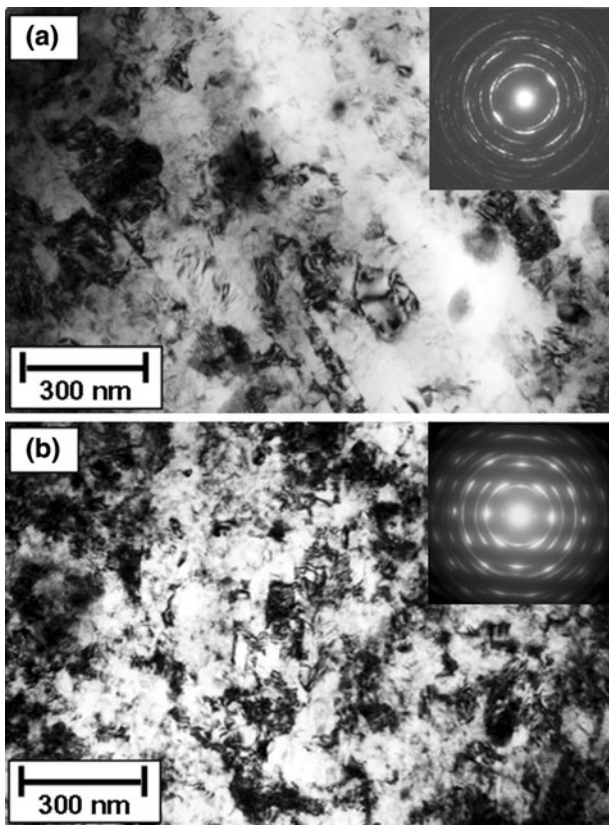


Fig. 8—TEM micrographs and SAED patterns of samples processed for (a) 10 revolutions under 2 GPa with rotation speed of 1.0 rpm and (b) 10 revolutions under 6 GPa with rotation speed of 0.2 rpm.

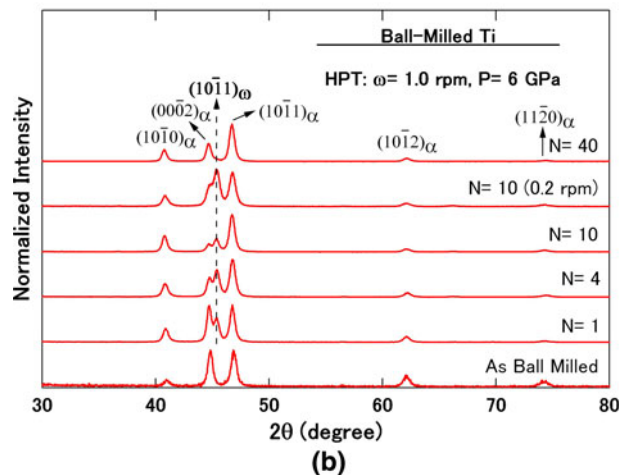
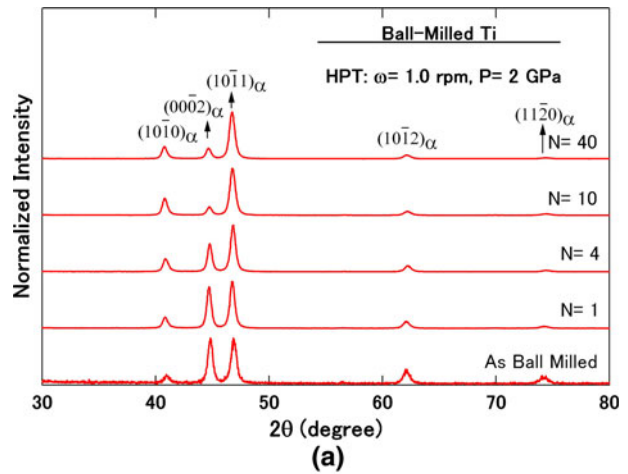


Fig. 9—XRD profiles for samples processed after various revolutions under (a) 2 GPa and (b) 6 GPa.

IV. DISCUSSION

Earlier studies showed that the hardness variation is represented by a unique function of equivalent strain for bulk samples subjected to HPT.^[46,47,49–54] The hardness behavior of Ti powders consolidated with HPT, as shown in Figure 3, is then essentially similar to that of the bulk Ti after HPT.^[46] The following two points should be noted from the comparison between the results of bulk and powders after HPT processing.

First, the saturation level at the steady state for the powders is higher than that for the bulk by ~70 Hv. It is considered that this difference can be due to contamination oxidation or straining during the BM process for the powders. To clarify this, additional results for powder and bulk samples without BM both with the same purity as 99.9 pct was shown in Figure 10. Both tensile and bending strengths are higher for the HPT-consolidated powder samples than the bulk samples. This indicates that oxide layers on the Ti powders contribute to an appreciable enhancement of the strength as a reinforcement after consolidation by HPT. These observations are consistent with an earlier article reporting that the oxidation of the Ni powders has a large effect on the grain refinement, the mechanical

fraction of ω phase increases with increasing strain.^[43–46] However, the peak height of ω phase decreases for $N = 10$ and disappears by $N = 40$.

- (5) For the samples subjected to HPT under 6 GPa for $N = 10$, the peak height of ω phase increases with a decrease in the rotation speed from 1.0 to 0.2 rpm.

Figure 10 delineates (a) the nominal stress-displacement curves obtained from the bending tests and (b) the nominal stress-strain curves obtained from the tensile tests at room temperature for two reference HPT-processed samples: first, powder sample without BM with the purity of 99.9 pct; and second, a bulk sample with the same purity of 99.9 pct. Both tensile and bending strengths are higher and tensile and bending ductilities are less for the HPT-consolidated powder samples than the bulk samples. The bulk sample processed with HPT bent to a hairpin shape confirming an excellent ductility, and this is even comparable with the ductility of the annealed sample, as reported earlier.^[51]

The density measurement in this study revealed that an average density of $4.543 \pm 0.009 \text{ g}\cdot\text{cm}^{-3}$ was obtained after cold consolidation with HPT for 10 revolutions under 2 GPa. Since the density for the annealed bulk sample was measured $4.549 \text{ g}\cdot\text{cm}^{-3}$ in this study, a relative density as high as 99.9 pct is attained following the HPT, indicating an almost perfect consolidation free of porosity.

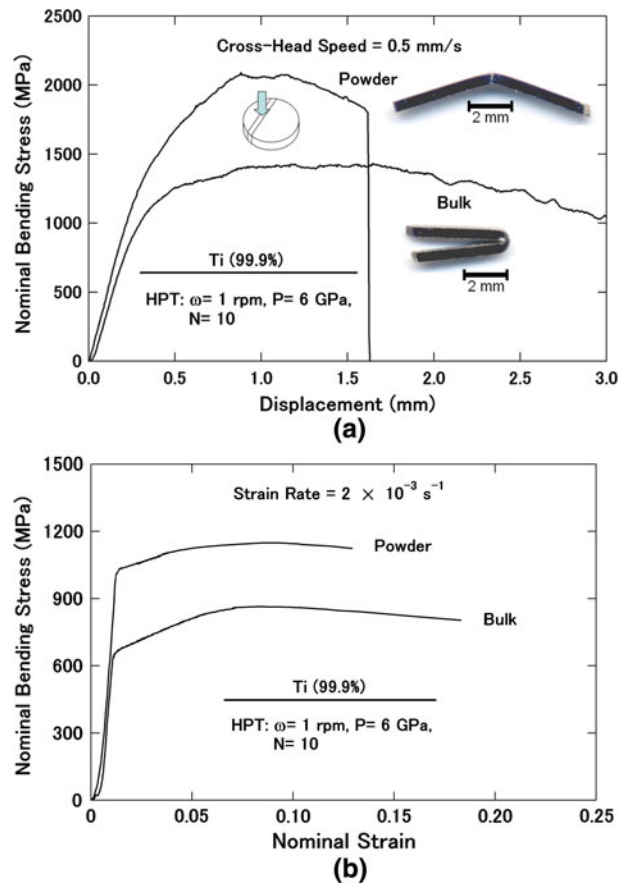


Fig. 10—(a) nominal bending stress vs displacement curves in pressing direction and (b) nominal tensile stress vs nominal strain curves for Ti powders and bulk sample processed for $N = 10$ revolutions under 6 GPa with rotation speed of 1.0 rpm.

properties, and the thermal stability of the consolidated material due to pinning effect of the oxide particles.^[21] When Figure 10 is compared with Figures 4 and 5, the strength of both bending and tensile tests are appreciably higher in the ball-milled powders than in the powders without BM. Thus, contamination or straining during BM appear to be other causes for the enhancement of the strength. It should be noted that HPT was conducted under 6 GPa in this additional experiment, but XRD analysis confirmed that the transformation to ω phase was not detected because of the rotation speed, which is high enough to raise the temperature during HPT processing and, thus, to induce the reverse transformation to α phase, as discussed subsequently.

Second, the saturation level of hardness depends not only on the applied pressure but also on the numbers of revolutions and rotation speeds, as reported on the bulk.^[46] The higher hardness obtained under 6 GPa is due to the formation of the ω phase through the $\alpha \rightarrow \omega$ phase transformation during HPT processing, as shown in Figure 9. The formation of the ω phase and its stability with respect to strain were described in detail earlier.^[46] The deviation to lower hardness levels shown in Figure 3(b) must be due to heat generation and a reverse transformation from the ω phase to the α phase during HPT processing. Because the rotation speed is as

high as 1.0 rpm and/or the number of revolutions is as large as $N = 10$ and 40, the heat generation is sufficient enough to introduce the reverse transformation, as shown in Figure 9(b). It was confirmed that the anvil temperature recorded during HPT at 6 GPa reached 331 K (58 °C) and 354 K (81 °C) for 10 and 40 revolutions, respectively, with a rotation speed of 1.0 rpm. Considering the fact that the thermocouple was located 10 mm away from the sample, it is reasonable that the sample temperature may be increased enough to cause a reverse phase transformation and, thus, to lower the hardness. For the sample processed under 6 GPa for $N = 10$ with a rotation speed of 0.2 rpm, heat generation was insignificant and, thus, the temperature reached 307 K (34 °C), which was not high enough for reverse transformation. Therefore, the peak height for the ω phase, as shown in Figure 9(b), and the hardness level, as shown in Figure 3(a), are well higher for the rotation speed of 0.2 rpm than that of 1.0 rpm.

The results of bending and tensile tests shown in Figures 4 and 5 demonstrate that high strength and reasonable ductility are achieved after cold consolidation of powders using HPT. The lower ductility for the samples processed at 6 GPa in Figure 5(b) must be a result of the ω -phase formation, which is more brittle than the α phase. Examination of Figures 5 through 7 indicates the following two important points. First, the highest ductility and strength as well as the finest dimplelike pattern fracture surface is achieved for the sample subjected to 40 revolutions under 6 GPa. Therefore, the transformation of α phase to ω phase and the full reverse transformation of ω phase to α phase lead to promising mechanical properties in HPT-consolidated ball-milled Ti. Similar behavior is expected for the bulk sample following HPT under 6 GPa and large numbers of revolutions or following post-HPT annealing at temperatures slightly higher than the reverse transformation temperature from ω phase to α phase (>223 K (150 °C)^[46]). Second, the numbers of revolutions for achieving the maximum strength and ductility is 10 under 2 GPa, as shown in Figure 5(a), indicating that the consolidation is completed after 10 revolutions. However, the maximum strength is achieved after 4 revolutions under 6 GPa, as in Figure 5(b). Therefore, higher applied pressure gives rise to more expeditious consolidation in consistence with earlier reports that a higher density is achieved at higher pressures for composite powders.^[11,12] For the sample consolidated with HPT for $N = 40$ under 2 GPa, the sample fractured in a brittle manner despite the fact that the sample contains no ω phase. OM observations indicate that this brittle fracture can be due to the formation of cracks during processing by HPT for $N = 40$, as reported in a Mg alloy.^[55]

Figure 11 shows summary of the tensile tests after BM followed by HPT of Ti powders together with relevant published data for comparison.^[41,46,56–58] The published data include those after annealing, cold rolling, or hot rolling of bulk Ti^[41,46] and of bulk Ti-6 pct Al-4 pct V,^[41] HPT of bulk Ti under 2 and 6 GPa,^[46] equal-channel angular pressing (ECAP) of bulk Ti for 8 passes,^[56,57] ECAP followed by cold rolling

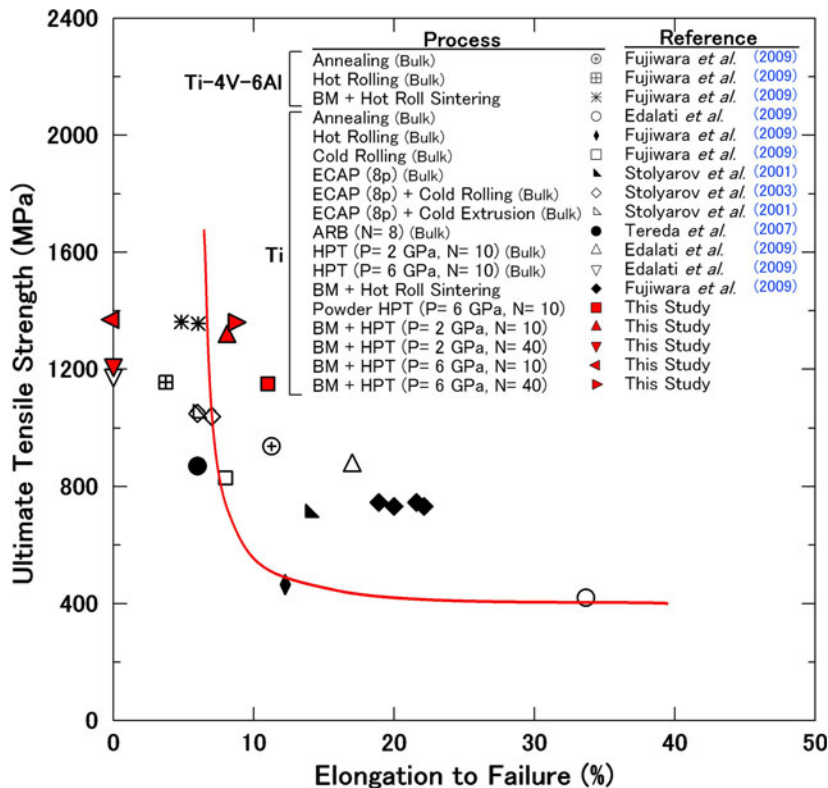


Fig. 11—Plots of ultimate tensile strength vs elongation to failure including published data for samples of pure Ti and Ti-6 pct Al-4 pct V after processing with different methods.^[41,46,56–58]

or cold extrusion,^[56,57] accumulative roll-bonding of bulk Ti for 8 passes,^[58] and of BM followed by hot roll sintering of Ti powders.^[41] Solid line represents a relation delineated through the points obtained by the annealed sample and conventional cold-rolled and hot-rolled samples for bulk Ti. It should be noted that, as pointed out by Zhao *et al.*,^[59] care is required for this comparison, because the ratios of the gage length to the gage width are varied from 1 to 5. There is a trade-off relation between the strength and the elongation to failure for all data points plotted in Figure 11. However, HPT processing in the optimized conditions ($N = 40$ under 6 GPa and $N = 10$ under 2 GPa) provides important advantages over hot roll sintering. First, the strength of pure Ti is significantly enhanced so that it becomes comparable to the strength of Ti-6 pct Al-4 pct V after severe plastic deformation with even better ductility when ball-milled powders are used. Second, bulk Ti increases its strength over the strength of Ti ball-milled and sintered powders. Third, HPT processing can successfully achieve dense consolidation without requiring heating either of the powders or of the processing system. It is found that Ti processed by BM followed by HPT shows the highest strength when compared to other processing methods, as shown in Figure 11.

V. SUMMARY AND CONCLUSIONS

Ball-milled pure Ti powders were consolidated by HPT and the following conclusions were obtained.

1. The hardness variation can be represented as a unique function of equivalent strain for powders consolidated with HPT.
2. A relative density as high as 99.9 pct, a high tensile strength of 1.35 GPa, a reasonable ductility of 8 pct, and an average grain size of ~ 150 nm are achieved after cold consolidation using HPT for 10 revolutions.
3. In HPT processing, higher applied pressure and strain give rise to more expeditious consolidation.
4. A phase transformation occurs from α phase to ω phase during HPT under 6 GPa, whereas no phase transformation is detected after processing with BM alone.
5. Transformation of α phase to ω phase and full reverse transformation of ω phase to α phase improves the mechanical properties of consolidated powders.
6. Both strength and ductility of pure Ti processed with BM followed by HPT are well comparable to those of Ti-6 pct Al-4 pct V after severe plastic deformation, indicating no requirement of alloying elements.

ACKNOWLEDGMENTS

We thank Professor Kenji Higashida, Kyushu University, for permitting the use of the bending test facility, and Dr. Masaki Tanaka, Kyushu University, for helpful assistance in using a bending test machine.

We are also grateful to Professor H. Miura, Kyushu University, for lending us a facility of the density measurement. One of the authors (KE) thanks the Islamic Development Bank for a scholarship. This work was supported, in part, by a Grant-in-Aid for Scientific Research from the Ministry of Education, Culture, Sports, Science and Technology of Japan in the Priority Area “Giant Straining Process for Advanced Materials Containing Ultra-High Density Lattice Defects” and, in part, by Kyushu University Interdisciplinary Programs in Education and Projects in Research Development (P&P).

REFERENCES

- R.Z. Valiev, R.K. Islamgaliev, and I.V. Alexandrov: *Prog. Mater. Sci.*, 2000, vol. 45, pp. 103–89.
- A.V. Korznikov, I. Safarov, D.V. Laptionok, and R.Z. Valiev: *Acta Metall. Mater.*, 1991, vol. 39, pp. 3193–97.
- V.A. Zilbershtein, N.P. Chistotina, A.A. Zharov, N.S. Grishina, and E.I. Estrin: *Fiz. Metal. Metalloved.*, 1975, vol. 39, pp. 445–47.
- P.W. Bridgman: *Phys. Rev.*, 1935, vol. 48, pp. 825–47.
- H. Shen, B. Guenther, A.V. Koanikov, and R.Z. Valiev: *Nanostruct. Mater.*, 1995, vol. 6, pp. 385–88.
- R.Z. Valiev, R.S. Mishra, J. Groza, and A.K. Mukherjee: *Scripta Mater.*, 1996, vol. 34, pp. 1443–48.
- J. Sort, A.P. Zhilyaev, M. Zielinska, J. Noguees, S. Surinach, J. Thibault, and M.D. Baro: *Acta Mater.*, 2003, vol. 51, pp. 6385–93.
- Z. Lee, F. Zhou, R.Z. Valiev, E.J. Lavernia, and S.R. Nutt: *Scripta Mater.*, 2004, vol. 51, pp. 209–14.
- I.V. Alexandrov, Y.T. Zhu, T.C. Lowe, R.K. Islamgaliev, and R.Z. Valiev: *Nanostruct. Mater.*, 1998, vol. 10, pp. 45–54.
- I.V. Alexandrov, Y.T. Zhu, T.C. Lowe, and R.Z. Valiev: *Powder Metall.*, 1998, vol. 41, pp. 11–13.
- I.V. Alexandrov, Y.T. Zhu, T.C. Lowe, R.K. Islamgaliev, and R.Z. Valiev: *Metall. Mater. Trans. A*, 1998, vol. 29A, pp. 2253–60.
- V.V. Stolyarov, Y.T. Zhu, T.C. Lowe, R.K. Islamgaliev, and R.Z. Valiev: *Mater. Sci. Eng. A*, 2000, vol. 282, pp. 78–85.
- R. Kuzel, Z. Matej, V. Cherkaska, J. Pesicka, J. Cizek, I. Prochazka, and R.K. Islamgaliev: *J. Alloys Compd.*, 2004, vol. 378, pp. 242–47.
- R.K. Islamgaliev, W. Buchgraber, Y.R. Kolobov, N.M. Amirkanov, A.V. Sergueeva, K.V. Ivanov, and G.P. Grabovetskaya: *Mater. Sci. Eng. A*, 2001, vols. 319–321, pp. 872–76.
- T. Tokunaga, K. Kaneko, and Z. Horita: *Mater. Sci. Eng. A*, 2008, vol. 490, pp. 300–04.
- T. Tokunaga, K. Kaneko, K. Sato, and Z. Horita: *Scripta Mater.*, 2008, vol. 58, pp. 735–38.
- E. Menendez, J. Sort, V. Langlais, A. Zhilyaev, J.S. Munoz, S. Surinach, J. Noguees, and M.D. Baro: *J. Alloys Compd.*, 2007, vols. 434–435, pp. 505–08.
- E. Menendez, G. Salazar-Alvarez, A.P. Zhilyaev, S. Surinach, M.D. Baro, J. Noguees, and J. Sort: *Adv. Funct. Mater.*, 2008, vol. 18, pp. 3293–98.
- H. Li, A. Misra, Y. Zhu, Z. Horita, C.C. Koch, and T.G. Holesinger: *Mater. Sci. Eng. A*, 2009, vol. 523, pp. 60–64.
- H. Li, A. Misra, Z. Horita, C.C. Koch, N.A. Mara, P.O. Dickerson, and Y. Zhu: *J. Appl. Phys.*, 2009, vol. 95, p. 071907.
- A. Bachmaier, A. Hohenwartera, and R. Pippan: *Scripta Mater.*, 2009, vol. 61, pp. 1016–19.
- W.J. Botta Filho, J.B. Fogagnolo, C.A.D. Rodrigues, C.S. Kiminami, C. Bolfarini, and A.R. Yavari: *Mater. Sci. Eng. A*, 2004, vols. 375–377, pp. 936–941.
- J. Sort, D.C. Ile, A.P. Zhilyaev, A. Concustell, T. Czeppe, M. Stoica, S. Surinach, J. Eckert, and M.D. Baro: *Scripta Mater.*, 2004, vol. 50, pp. 1221–25.
- A.R. Yavari, W.J. Botta Filho, C.A.D. Rodrigues, C. Cardoso, and R.Z. Valiev: *Scripta Mater.*, 2002, vol. 46, pp. 711–16.
- Z. Kovacs, P. Henits, A.P. Zhilyaev, and A. Revesz: *Scripta Mater.*, 2006, vol. 54, pp. 1733–37.
- N. Boucharat, R. Hebert, H. Rosner, R.Z. Valiev, and G. Wilde: *J. Alloys Compd.*, 2007, vols. 434–435, pp. 252–54.
- T. Czeppe, G. Korznikova, J. Morgiel, A. Korznikov, N.Q. Chinh, P. Ochin, and A. Sypien: *J. Alloys Compd.*, 2009, vol. 483, pp. 74–77.
- K. Edalati, Y. Yokoyama, and Z. Horita: *Mater. Trans.*, 2010, vol. 51, pp. 23–26.
- A.P. Zhilyaev, A.A. Gimazov, G.I. Raab, and T.G. Langdon: *Mater. Sci. Eng. A*, 2008, vol. 486, pp. 123–28.
- A.P. Zhilyaev, S. Swaminathan, A.A. Gimazov, T.R. McNelley, and T.G. Langdon: *J. Mater. Sci.*, 2008, vol. 43, pp. 7451–56.
- K. Edalati and Z. Horita: *Scripta Mater.*, 2010, vol. 63, pp. 174–77.
- J.S. Benjamin: *Sci. Am.*, 1976, vol. 234, pp. 40–48.
- C. Suryanarayana: *Prog. Mater. Sci.*, 2001, vol. 46, pp. 1–184.
- ASM Handbook*, vol. 7, *Powder Metal Technologies and Applications*, 10th ed., ASM INTERNATIONAL, Metals Park, OH, 1998.
- C.J. Lu, J. Zhang, and Z.Q. Li: *J. Alloys Compd.*, 2004, vol. 381, pp. 278–83.
- Y.Y. Li, C. Yang, W.P. Chen, X.Q. Li, and M. Zhu: *J. Mater. Res.*, 2007, vol. 22, pp. 1927–32.
- P. Chatterjee and S.P. Sen Gupta: *Philos. Mag. A*, 2001, vol. 81, pp. 49–60.
- I. Manna, P.P. Chattopadhyay, P. Nandi, F. Banhart, and H.J. Fecht: *J. Appl. Phys.*, 2003, vol. 93, pp. 1520–24.
- J. Dutkiewicz, J. Kusnier, M. Maziarz, M. Lejkowska, H. Garbacz, M. Lewandowska, A. Dobromyslov, and K.J. Kurzydowski: *Phys. Status Solidi A*, 2005, vol. 202, pp. 2309–20.
- F. Sun, A. Zuniga, P. Rojas, and E.J. Lavernia: *Metall. Mater. Trans. A*, 2006, vol. 37A, pp. 2069–78.
- H. Fujiwara, T. Sekiguchi, and K. Ameyama: *Int. J. Mater. Res.*, 2009, vol. 100, pp. 796–99.
- Y.K. Vohra, S.K. Sikka, S.N. Vaidya, and R. Chidambaran: *J. Phys. Chem. Solids*, 1977, vol. 38 (11), pp. 1293–96.
- A.R. Kilmametov, A.V. Khristoforova, G. Wilde, and R.Z. Valiev: *Z. Kristallogr. Suppl.*, 2007, vol. 26, pp. 339–44.
- Y. Ivanisenko, A. Kilmametov, H. Rosner, and R.Z. Valiev: *Int. J. Mater. Res.*, 2008, vol. 99, pp. 36–41.
- Y. Todaka, J. Sasaki, T. Moto, and M. Umamoto: *Scripta Mater.*, 2008, vol. 59, pp. 615–18.
- K. Edalati, E. Matsubara, and Z. Horita: *Metall. Mater. Trans. A*, 2009, vol. 40A, pp. 2079–86.
- K. Edalati, Z. Horita, S. Yagi, and E. Matsubara: *Mater. Sci. Eng. A*, 2009, vol. 523, pp. 277–81.
- ASTM E290, *Standard Test Methods for Bend Testing of Material for Ductility*, ASTM International, West Conshohocken, PA, 2009.
- K. Edalati, Z. Horita, and T.G. Langdon: *Scripta Mater.*, 2009, vol. 60, pp. 9–12.
- K. Edalati, T. Fujioka, and Z. Horita: *Mater. Trans.*, 2009, vol. 50, pp. 44–50.
- K. Edalati, Z. Horita, M. Tanaka, and K. Higashida: *Adv. Mater. Res.*, 2010, vols. 89–91, pp. 171–76.
- A. Vorhauer and R. Pippan: *Scripta Mater.*, 2004, vol. 51, pp. 921–25.
- K. Edalati, T. Fujioka, and Z. Horita: *Mater. Sci. Eng. A*, 2008, vol. 497, pp. 168–73.
- K. Edalati, Z. Horita, and Y. Mine: *Mater. Sci. Eng. A*, 2010, vol. 527, pp. 2136–41.
- M. Kai, Z. Horita, and T.G. Langdon: *Mater. Sci. Eng. A*, 2008, vol. 488, pp. 117–24.
- V.V. Stolyarov, Y.T. Zhu, T.C. Lowe, and R.Z. Valiev: *Mater. Sci. Eng. A*, 2001, vol. 303, pp. 82–89.
- V.V. Stolyarov, Y.T. Zhu, I.V. Alexandrov, T.C. Lowe, and R.Z. Valiev: *Mater. Sci. Eng. A*, 2003, vol. 343, pp. 43–50.
- D. Terada, S. Inoue, and N. Tsuji: *J. Mater. Sci.*, 2007, vol. 42, pp. 1673–81.
- Y.H. Zhao, Y.Z. Guo, Q. Wei, A.M. Dangelewicz, C. Xu, Y.T. Zhu, T.G. Langdon, Y.Z. Zhou, and E.J. Lavernia: *Scripta Mater.*, 2008, vol. 59, pp. 627–30.